Co diffusion in the near-surface region of Cu

T. Siahaan, O. Kurnosikov, H. J. M. Swagten, and B. Koopmans
Department of Applied Physics, Eindhoven University of Technology, 5600 MB Eindhoven, The Netherlands

S. V. Kolesnikov, A. M. Saletsky, and A. L. Klavsyuk
Faculty of Physics, Moscow State University, 119991 Moscow, Russian Federation

(Received 30 June 2016; revised manuscript received 27 September 2016; published 23 November 2016)

We present our experimental and theoretical study on Co diffusion in the first few atomic layers of Cu(001). While the diffusion of Co atoms in Cu(001) is usually expected to be intense at a temperature $T \geqslant 800$ K, in the vicinity of the surface, it is already activated at a considerably lower temperature $T \sim 650$ K whereas the diffusion in the deep bulk region is still inhibited. This intense near-surface diffusion provides an accumulation of Co atoms in the first six atomic layers upon a single stage Co deposition. The details of the near-surface diffusion are studied by analyzing the distribution of the location depth of the buried single Co atoms. The depth of location of single Co atoms is deduced from scanning tunneling microscopy (STM) data. The subsurface Co atoms induce a perturbation of the electron density of states of the surface which is observable as apparent ringlike ripples in the STM images of the atomically flat Cu surface. The depth of location of the buried Co atoms is determined from the diameter of those rings. The largest amount of Co atoms is found to be in the third layer, emphasizing that the near-surface diffusion should be described by diffusion parameters different from those for bulk diffusion. A model that describes the embedding process of Co atoms into Cu(001) layers is developed. The model assumes Co atoms to diffuse via the vacancy and ring-exchange mechanisms. The energy barriers for the interlayer Co diffusion via those mechanisms are calculated using the nudged elastic band method. The model satisfactorily explains the experimental results. Our study reveals that the energy barriers for Co diffusion in the first five atomic layers of Cu(001) are lower than those in the bulk. This defines the region in which Co diffusion should be considered as a near-surface one.

DOI: 10.1103/PhysRevB.94.195435

I. INTRODUCTION

Studies on atomic diffusion in solids, thin-film growth, and subsurface nanoclusters show that diffusion in the vicinity of the surface can not always be explained by implementing the bulk values of diffusion parameters [1–15]. This implies that the process of diffusion is affected by the proximity of the surface. The discrepancy between the diffusion in the near-surface region and in the deep bulk raises the following question: until what depth the proximity of the surface affects this process? This question is addressed in the present work for the case of near-surface diffusion of single Co atoms in Cu(001). The near-surface diffusion is considered important, for example, in the thin-film technology where it results in intermixing at the interface.

Despite the fact that the Co-Cu(001) system has been studied extensively, studies on Co diffusion were done mainly for the diffusion *on the surface*, *into*, and *across the first layer*, as well as *in the deep bulk*. They provide the surface and bulk values of the diffusion parameters that have been reported elsewhere [16–25]. On the other hand, Co diffusion in the region close to the Cu(001) surface has rarely been investigated. Here, we present a detailed study on this near-surface process, and show how the values of Co diffusion parameters vary in the near-surface region and converge towards their bulk values.

The experiment to study the near-surface diffusion requires a condition where it can be easily distinguished from the bulk diffusion. This requirement is met when the diffusion in the near-surface region is intense while being inhibited in the deep bulk. Since diffusion is thermally activated, achieving this condition needs a careful determination of the experimental temperature. Diffusion is considered intense when the rate of atomic jumps is sufficiently high, which is higher than $\sim$1 min^{-1} regarding our experiment. The rate of atomic jumps f is determined by the temperature T via the relation

$$f = f_0 \exp\left(-\frac{Q}{kT}\right), \tag{1}$$

where Q is the energy barrier of the atomic jump, k is the Boltzmann constant, and f_0 is the attempt frequency, which is assumed to be equal to the Debye frequency. The activation energy for the jump of a Co atom into the first layer of Cu(001) is up to $\sim$1 eV [19–21]. Implementing this value into Eq. (1), one can deduce that the diffusion into the first layer is intense at $T \gtrsim 350$ K [16–21]. Considering the activation energy of the jump of a Co atom in bulk Cu $E_b = 2.22$ eV [24], an intense bulk diffusion should be achieved only at a much higher temperature $T \geqslant 800$ K. Assuming the proximity to the surface facilitates Co diffusion, the temperature range that meets the requirement of our experiment should be expected to lie in between 350 and 800 K. The experimental evidences that validate this prediction can be found in previous reports. Co depositions on Cu(001) at 540 and 650 K result in the self-burying of Co below the surface as reported in Refs. [13,14]. Although not established in Ref. [13], in Ref. [14], this burying process is attributed to the near-surface diffusion. Yet neither the mechanisms nor the corresponding physical parameters are in the scope of those reports. Bulk diffusion

in those experiments should be insignificant as the rate of jumps of Co atoms in bulk Cu is lower than 3×10^{-2} min^{-1} at the experimental temperatures. Considering this, one can deduce that the temperature range of 540–650 K provides the condition that is required in our experiment on the near-surface diffusion.

Based on the discussion above, we performed the experiment by depositing Co on a Cu(001) substrate at 650 K. We experimentally found that Co atoms do not stay on or in the first layer of the substrate upon such a deposition. Instead, they diffuse into the subsurface region and accumulate in the first few subsurface atomic layers of the substrate. To study the details of that diffusion, the distribution of the depth of the location of the buried Co atoms is analyzed. The depth of location of single Co atoms was determined using scanning tunneling microscopy (STM) [26,27]. The distribution of the depth of location reveals that the largest amount of Co atoms is in the third layer. Our experimental findings could not be explained if Co diffusion in the first few subsurface layers were described using the surface or the bulk values of Co diffusion parameters. To provide an explanation for the experimental results, a theoretical work that elucidates Co *near-surface* diffusion in Cu(001) was carried out. A model that describes Co diffusion in the near-surface region of Cu(001) is proposed where realistic diffusion mechanisms are presented. To our knowledge, such a modeling was either never or only done incompletely in previous reported works. The energy barriers for Co diffusion in the first few layers of Cu(001) as well as in the deep bulk have been calculated. Using the model, the experimental results are well explained.

This paper is organized as follows. The general description of the experiment is given in the next section. In Sec. III, the burying of Co atoms and the distribution of Co in Cu(001) are presented and discussed. The theoretical modeling is presented in Sec. IV. The comparison between the experimental and theoretical results is given in Sec. V. Section VI summarizes this report.

II. EXPERIMENT

The experiment was performed in an ultrahigh vacuum system with a low-temperature STM (LT-STM) (Omicron). The samples were fabricated and analyzed *in situ*. The sample with Co atoms embedded in it was obtained by depositing a small amount of Co [<0.1 monolayers (ML)] on a Cu(001) substrate at 650 K. Before the deposition, the substrate was cleaned using a standard sputtering-annealing procedure. The deposition rate was ~0.2 ML min^{-1} and the base pressure was $<5 \times 10^{-10}$ mbar. After the deposition, the sample was cooled down in ~30 min to reach the room temperature before being introduced into the LT-STM.

The sample was characterized using STM. The measurements were performed at 78 K with a base pressure $<10^{-10}$ mbar. The STM imaging was done at the constant-current mode, providing topographic maps of the samples surface. The buried Co atoms induce specific features that are observed in the STM images. The detailed description of the features is given in the next section. These features are used to determine the location of the subsurface Co atoms.

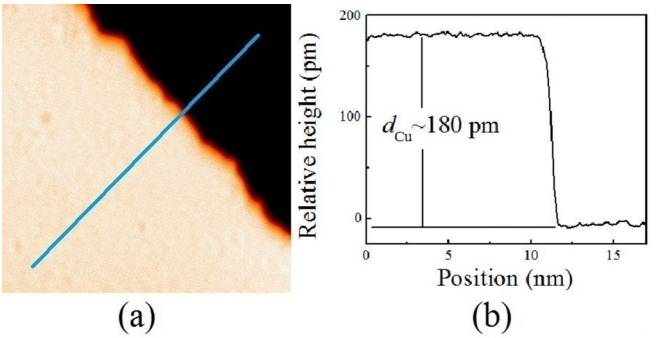

FIG. 1. (a) The topographic map of the Cu(001) surface, 15 × 15 nm^2, after the deposition of Co at 650 K. The areas with different contrasts are two atomically flat terraces. (b) The surface profile along the line in (a). A single atomic step between the atomically flat terraces is shown in the image.

III. EXPERIMENTAL RESULTS AND DISCUSSION

A. Burying of Co atoms below the Cu(001) surface

Figure 1(a) presents a typical STM image of Cu(001) after the deposition of <0.1 ML Co. It shows two atomically flat terraces with a height difference ~180 pm, corresponding to the interlayer spacing in Cu(001) d_{Cu} [Fig. 1(b)]. The topographic maps reveal no islands on the surface. Moreover, we did not observe Co atoms embedded in the first layer. Co atoms that were embedded in the first layer should have been observed as protrusions in the STM images of the atomically flat terraces acquired at a bias voltage in the range between −2.5 and +2.5 eV [16,19,28–31]. Since such protrusions were never observed in our measurements, we conclude that there should be almost no Co atoms embedded in the first layer. All of these confirm that at 650 K Co atoms neither stay on the surface nor in first layer of Cu(001). Instead, they go into the region below the first layer as was also reported previously [13,14,32].

Nevertheless, the STM images of the atomically flat terraces are not exactly the same as those of a clean Cu(001) substrate that contains no Co. The topographic maps of the samples with buried Co atoms reveal ripples on those terraces [Fig. 2(a)]. The ripples are of ringlike shape with their diameter ranging

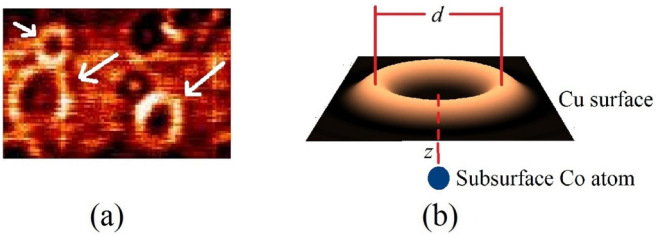

FIG. 2. (a) The ringlike ripples observed in the STM images of the atomically flat terraces after the deposition at 650 K. The arrows show rings with different diameters, corresponding to different location depths of the single Co atoms. The image shows an area of 6.25 × 4.06 nm^2. The tunneling set point is (−0.15 V,1 nA). (b) The simulated illustration of the relation between the depth of a buried Co atom, z, and the diameter of the ripple above it, d. The Co atom is represented by the dark blue sphere.

from ∼0.5 to ∼2.0 nm. In principle, the apparent ringlike ripples could be induced by surface impurity atoms. Impurity atoms that are embedded in the first layer scatter surface electrons, inducing oscillations of the electron density of states at the surface that are imaged as concentric ripples in the STM images. Such oscillations are mainly observed in the STM images of surfaces that provide 2D electron states associated with the surface states. This situation is well known for Cu(111) [33–36]. Unlike the case of Cu(111), the STM images of Cu(001) show no oscillations of surface electron density of states that are induced by surface impurities. Moreover, the apparent ringlike ripples that are induced by surface impurities always show several periods of oscillations which were never revealed in our experiments. Therefore the ringlike ripples that are observed in our measurements should not be attributed to the surface impurity atoms.

The apparent ringlike ripples that are observed in our experiment are similar to those observed by Weismann *et al.* in the STM images of the atomically flat Cu(001) and Cu(111) surfaces with single Co atoms buried below them [26]. They are due to the perturbed surface electron density of states, which is caused by the subsurface scattering of substrate electrons. The subsurface Co impurities act as scattering centers [26,27,37]. The shape of the ripples in general is nearly circular, while the exact shape is determined by the electronic band structure of Cu. Thus the ringlike ripples that are observed in our experiment identify single Co atoms that are hidden below the Cu surface.

The remarkable self-burying of Co atoms below the surface at the temperature of 650 K would not be expected if the properties of the second and deeper layers of Cu(001) were assumed to be the same as those of the deep bulk. Considering the low-energy barrier for the incorporation of a Co atom from the surface into the first layer, which is only up to ∼1 eV [20,21], this process takes less than 10 μs at our deposition temperature as deduced using Eq. (1). With an energy barrier of $E_b = 2.22$ eV, the typical time required for a Co atom to jump from one into another lattice point in the bulk Cu at 650 K is ∼7 hours. Taking into account the deposition rate and the experimental time scale, Co would have accumulated in the first layer if the energy barriers for the diffusion into the second and deeper atomic layers were equal to E_b. This is in contrast with our observation which reveals no Co atoms in the first layer after a deposition on a hot Cu(001). It means the energy barrier for Co diffusion in the near-surface region should be lower than E_b, providing the accumulation of Co atoms into that region.

The conclusion above implies that the energy barrier for Co diffusion in Cu(001) is depth dependent. Since the rate of Co migration into different depths is determined by the energy barrier for diffusion, the distribution of the depth of location of the buried Co atoms reflects this depth dependency of the barrier. The discussion and further data about the depth distribution are presented in the following section.

B. Co distribution in Cu(001)

The distribution of the depth of location of the buried Co atoms is determined by analyzing the apparent ringlike ripples similar to those in Fig. 2(a). As shown by Weismann *et al.*, the size of each apparent ring corresponds to the depth of location of the impurity atom [26,27]. In general, the shape as well as the relation between the size of the specific ripple structures and the depth of the impurities can be complicated, depending on the band structure of the host material. Particularly for an impurity in Cu(001), the characteristic ripple structure has a roughly circular shape. The diameter of the ringlike ripple structure can be approximated by a simple formula [26] [Fig. 2(b)]:

$$d \approx 2z. \tag{2}$$

This formula was used to deduce the depth of location of the Co atoms in the Cu substrate from the diameter of the apparent rings revealed by STM images. The distribution of the depth of location of Co atoms is obtained by analyzing an ensemble of rings shown by STM data. To inspect the reproducibility of the resulting distribution, the analysis was carried out on two samples that were fabricated with a similar procedure.

The diameter of the ripples was measured along the ⟨100⟩ directions and calibrated to the atomically resolved images. The diameters are found to cluster around averaged values that differ by around a multiple integer of 360 pm with some variations of ∼100 pm (see the inset of Fig. 3). By applying

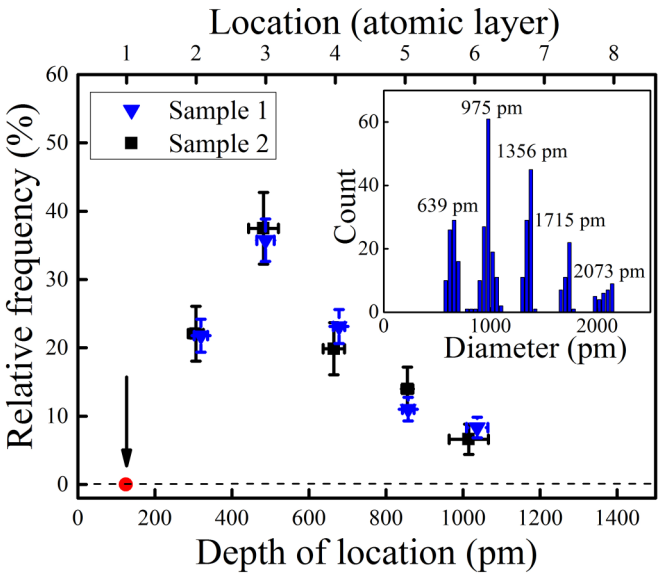

FIG. 3. The distribution of the location depth of Co atoms in Cu(001), deduced by analyzing STM data, where Eq. (2) has been implemented. Different symbols and colors (blue-filled triangles and black-filled squares) represent distributions obtained from different samples that were fabricated with a similar procedure. The horizontal error bars across the symbols show the standard deviation of the data distribution. The vertical ones represent the uncertainty of the relative counting frequency as derived from the counting uncertainty. The red-filled circle (pointed by the arrow) is an auxiliary point, showing the *estimated* depth of the center of atoms in the first atomic layer. The top of the horizontal axis presents the Cu(001) layers to which the depth is attributed. (Inset) The histogram of the distribution of the diameter of the apparent ringlike ripples. The diameters show a clustering around averaged values shown by the numbers above each cluster. The data presented by the histogram were analyzed to obtain the distribution presented by the blue-filled triangles.

Eq. (2) to the diameters in each cluster, the distributions of the depth of Co location are obtained as presented in Fig. 3. In the presentation of the distributions, the number of entries that correspond to each depth is normalized to the total number of entries in the corresponding data sets. The blue-filled triangles and the black-filled squares present two distributions that are obtained from the aforementioned two samples. Both distributions are consistent, showing the reproducibility of the observed distribution. To emphasize that there are almost no Co atoms embedded in the first layer, an auxiliary point is added in the plot as a red-filled circle (pointed by an arrow). The depth of this extra point corresponds to the *estimated* distance between the surface and the center of the atoms in the first layer, which is obtained by approximating the Cu atoms as hard spheres.

The distributions in Fig. 3 reveal that the depths of location of Co atoms differ by around the multiple integer of 180 pm. Such depth differences are correlated to the multiple integer of interlayer distance in Cu(001) d_{Cu}. Since Co atoms are very unlikely to form interstitials in Cu(001), they should be embedded in the atomic layers of the substrate. Based on this, the depths of location of Co atoms presented in the distributions are attributed to the layers of Cu(001).

The distributions of Co in Cu(001) reveal two main features. (1) The deposited Co atoms are embedded in the second up to the sixth atomic layers with almost no Co embedded in the first layer. (2) The largest number of Co atoms is in the third layer. The first feature is in good agreement with our previous report that shows efficient incorporation of Co in Cu(001) takes place in the region of ∼1 nm deep upon a deposition at 650 K [14].

The distribution maximum, which lies in the third layer, is a point for a deeper discussion. Simply assuming that the energy barrier for the diffusion in the near-surface layers monotonically increases towards the bulk value, one should expect the maximum of the distribution to lie at the first layer. The actual position of the distribution maximum implies that the depth dependency of the energy barrier for the diffusion is more complicated. To elucidate this depth dependency, the profile of the distribution is analyzed further where the factors that determine the distribution profile are considered.

C. Factors that determine Co distribution in Cu(001)

The distribution of Co in Cu(001) layers is determined by the rate of migration of Co atoms into those layers. The rate is dependent on the energy barriers of the interlayer migration via different mechanisms as well as the energetics of Co in Cu(001). The migration of Co atoms from one into another layer can take place via the vacancy as well as the ring-exchange mechanisms [38]. These mechanisms have different activation energy thus contributing differently to the overall migration rate. Moreover, the energy due to Co embedding in one layer of Cu(001) can be different from it in the other layers. Such difference of energy can result in the imbalances of the energy barriers for the interlayer migration.

Co migration via the vacancy mechanism occurs when one atom [Fig. 4(a)] or several neighboring atoms [Fig. 4(b)] shift their positions due to the jump of a vacancy. The probability that a Co atom migrates via this mechanism is determined by the chance that a vacancy meets the shifting atom(s), which

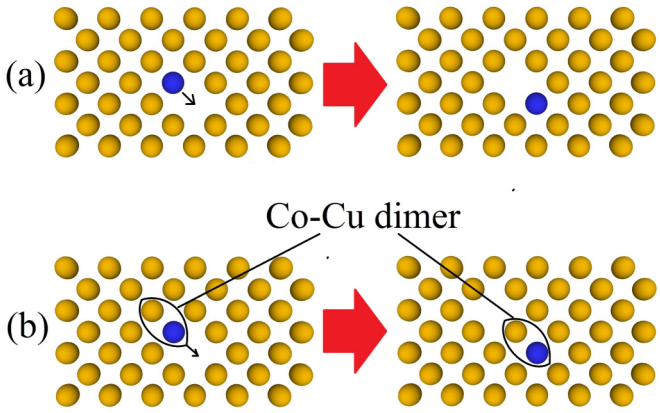

FIG. 4. The illustration of the diffusion via the vacancy mechanism. The Co atom is represented by the blue sphere while the Cu atoms by the orange ones. (a) A Co atom jumps into a vacancy. (b) A simultaneous shift of two neighboring atoms (a Co-Cu dimer) due to a vacancy jump.

depends on the concentration and the mobility of vacancies. These are given by the activation energy of vacancy diffusion E^{vac}, which is the sum of the vacancy formation energy E^{F} and migration energy E^{M},

$$E^{\mathrm{vac}} = E^{\mathrm{M}} + E^{\mathrm{F}}. \tag{3}$$

The concentration of vacancies in the subsurface of Cu(001) at the actual temperature in the experiment is very low. The vacancy concentration n can be estimated using the relation

$$n \sim \exp\left(-\frac{E^{\mathrm{F}}}{kT}\right). \tag{4}$$

In the bulk region, the reported experimental values of vacancy formation energy range from 1.17 ± 0.11 to 1.30 ± 0.05 eV [39–42]. This means the vacancy concentration in the deep bulk is less than 10^{-9}. In the first few subsurface layers, the vacancy formation energy can differ from the bulk value by $\leqslant 0.126$ eV as has been shown in a theoretical paper by Wang *et al.* [43]. Applying the values that are reported in Ref. [43] into Eq. (4) gives an estimated vacancy concentration of the same order as the concentration in the bulk. On the other hand, vacancies are very mobile in Cu at the experimental temperature. The mobility of vacancies is characterized by the migration energy. The reported experimental values of migration energy in the bulk region are in the range between 0.76 ± 0.04 and 0.91 ± 0.05 eV [39–42]. Near the surface, vacancy migration energy can differ from the bulk value by $\leqslant 0.05$ eV as shown in the calculation in Ref. [43]. Implementing these values of migration energy into Eq. (1) yields an estimated vacancy jump rate as high as in the order of 10^7 s^{-1}.

The migration via the ring-exchange mechanism occurs when two [Fig. 5(a)] or more [Fig. 5(b)] atoms exchange positions in a cyclic manner. The migration with this mechanism involves local elastic distortions of the substrate lattice, thus requires higher energies compared to the activation energy of the vacancy-assisted migration [38,44]. The elastic distortion energy decreases as the number of atoms that are involved in the exchange process increases. However, increasing the

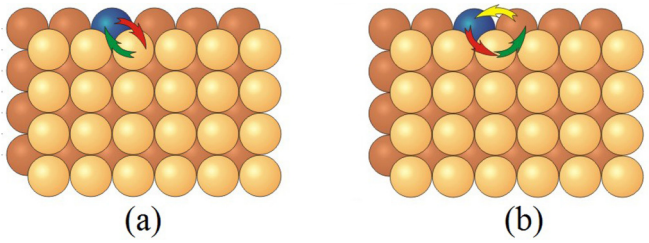

FIG. 5. The illustration of the migration of a Co atom via the exchange mechanism. The Co atom is represented by the blue spheres while Cu by the orange ones. (a) The exchange between a Co and a Cu atom. (b) The cyclic exchange that involves three atoms. Described by the picture is the cyclic exchange of a Co-Cu-Cu trimer in (111) plane.

number of the involved atoms requires higher correlation of the motion of the atoms, causing it very unlikely for an exchange that incorporates more than three or four atoms to take place [38]. In the bulk region, the cyclic-exchange process involves the local elastic deformation of the bulk lattice, causing the energy barrier for this process to be much higher than it is for the vacancy mechanism. In the near-surface region, the distortion involves less lattice points compared to it in the bulk process. This may lead to an energy barrier that is lower than the bulk value.

The energetics of the Co-Cu(001) system favors Co to be located below the first layer rather than on the surface or in the first layer [45,46]. A detail theoretical work by Levanov *et al.* shows that the locations of a single Co atom in the first two atomic layers of Cu(001) provide higher energies than the locations in the deeper layers [45]. In that work, they show that the difference of energy due to the embedding in the first and second layer is larger than it is due to the embedding in the second and deeper layers. These energy differences affect the apparent height of the barriers for the diffusion in the direction towards the bulk region and towards the surface. This results in imbalances in the migration from the second (third) layer into the first (second) layer and the migration in the other way around. To determine the actual imbalances, the energy barriers for the interlayer migration need to be calculated. This calculation is presented in the next section.

IV. MODELING

To understand the origin of the features shown in the experimental plot, the embedding of Co atoms into the layers of Cu(001) is modeled. In our model, the interlayer migration of Co atoms is described based on the discussion in Sec. III C. The migration of Co atoms is approximated as the migration of single Co atoms, which do not interact with each other because of the low concentration of Co atoms in the substrate in the actual experiment. The energy barriers for the interlayer migration are determined theoretically. The calculated energy barriers are used to calculate the rate of embedding of Co atoms into the layers of Cu(001) and the distribution of Co atoms in those layers upon the deposition at 650 K.

A. Description of the model

The embedding of Co atoms into the Cu substrate starts with the incorporation of the deposited atoms into the first layer. Taking into account the energy barrier for the embedding of a Co atom into the first layer of Cu(001), which is up to $\sim$1 eV [20,21], this process takes only <10 μs after a Co atom arrives on the 650-K Cu(001) as already mentioned in Sec. III A. This time is extremely short compared to the time scale of the experiment. Thus the embedding into the first layer is assumed to happen immediately once a Co atom lands on the hot surface.

The Co atoms in the first layer can actually go back to the surface. This process requires an energy which is higher by $\sim$0.5 eV compared to the energy barrier for the embedding into the first layer. The difference between these energy barriers is due to the different energy provided by the locations on the surface and in the first layer [45]. It results in the rate of the process of going back onto the surface being only $\sim 10^{-4}$ times the rate of the embedding process. Based on this, the process of Co atoms moving back from the substrate onto the surface is neglected.

The Co atoms that are embedded in the substrate undergo interlayer migration via the vacancy and the ring-exchange mechanisms. The migration via the vacancy mechanism takes place when a Co atom jumps into a neighboring vacancy or when a Co-Cu dimer moves due to a vacancy jump (see Fig. 4). To have these processes occurring, energies to form the vacancy and to have the vacancy jumping are required. The energy to form a vacancy in the jth layer of Cu(001) is E_j^{F}. The interaction between a vacancy and Co can lead to a different formation energy of a vacancy when Co is nearby. In the model, the Co-vacancy interaction is accommodated by a difference in the formation energy of a vacancy located next to a Co atom. The formation energy of a vacancy in the jth layer with the presence of a Co atom next to it in the $i = j \pm 1$-th layer is $E_j^{\mathrm{F}} + \Delta_{i,j}$. The energy barrier for the jump of a Co atom in the ith layer into an adjacent vacancy in the $j = i \pm 1$-th layer is $E_{i\to j}^{\mathrm{Co,vac}}$. The energy barrier for the migration via the shift of a Co-Cu dimer due to a vacancy jump is $E_{i\to j}^{\mathrm{dim,vac}}$.

The interlayer migration via the ring-exchange mechanism is assumed to involve not more than three atoms. The exchange that involves only a Co atom in the ith layer and a Cu atom in the $j = i \pm 1$-th layer has an energy barrier of $E_{\mathrm{i}\to j}^{\mathrm{Co,Cu}}$. The exchange involving three atoms is described as a cyclic exchange of a Co-Cu-Cu trimer in the (111) plane as described in Fig. 5(b). The energy barrier for the migration of a Co atom in the ith layer into the $j = i \pm 1$-th layer via this process is $E_{i\to j}^{\mathrm{trim}}$.

The model that is described above requires the energy parameters to be determined. For this, a theoretical work to determine the energy barriers for the processes that are considered in the model is carried out.

B. Calculation methods

To determine the parameters that characterize processes that are taken into account in the model description, the characteristic energies of the Co-Cu(001) system as well

TABLE I. Parameters of atomic potentials [49].

Parameter	Cu-Cu	Co-Co	Co-Cu
A^1 (eV)	0.0	0.0	−1.5520
A^0 (eV)	0.0854	0.1209	−0.0372
ξ	1.2243	1.5789	0.8522
p	10.939	11.3914	7.6226
q	2.2799	2.3496	5.5177
r_0 (Å)	2.5563	2.4953	2.4995

as the energy barriers for the Co migration are calculated. The characteristic energies of the Co-Cu(001) systems are calculated using the molecular statics simulation. The energy barriers are calculated using the nudged elastic band (NEB) method [47].

In the calculations, the interaction between atoms is described by the interatomic potentials formulated in the second moment of the tight-binding approximation [48]. This formulation has been demonstrated to be well applicable for the Co-Cu system [45,46,49–52]. The attractive term (the band energy), E_{B}^i, contains the many-body interaction. The repulsive term E_{R}^i is described by pair interactions (Born-Mayer form). The cohesive energy E_{C} is the sum of the attractive and the repulsive terms, i.e.,

$$E_{\mathrm{C}} = \sum_i \left(E_{\mathrm{R}}^i + E_{\mathrm{B}}^i\right), \tag{5}$$

$$E_{\mathrm{B}}^i = -\left\{\sum_{\mathrm{j}} \xi_{\alpha\beta}^2 \exp\left[-2q_{\alpha\beta}\left(\frac{r_{ij}}{r_0^{\alpha\beta}} - 1\right)\right]\right\}^{1/2}, \tag{6}$$

$$E_{\mathrm{R}}^i = \sum_{\mathrm{j}} \left[A_{\alpha\beta}^1\left(\frac{r_{ij}}{r_0^{\alpha\beta}} - 1\right) + A_{\alpha\beta}^0\right] \exp\left[-p_{\alpha\beta}\left(\frac{r_{ij}}{r_0^{\alpha\beta}} - 1\right)\right]. \tag{7}$$

Here, r_{ij} is the distance between the atoms i and j, α and β describe the type of atoms, $\xi_{\alpha\beta}$ is an effective hopping integral, $p_{\alpha\beta}$ and $q_{\alpha\beta}$ are parameters describing the decay of the interaction strength with the distance between atoms, while $r_0^{\alpha\beta}, A_{\alpha\beta}^0$, and $A_{\alpha\beta}^1$ are adjustable parameters of the interatomic interactions. The values of the parameters used in the calculations (see Table I) are taken from Ref. [49]. The fitting procedure is described in Ref. [45]. The reliability of the potentials for the case of Co atoms embedded in Cu(001) has been demonstrated in previous works [50–52].

The system of Co embedded in Cu(001) is simulated by a slab of atoms containing Co and Cu. The slab is twelve atomic layers thick and each layer consists of 4000 atoms. The position of the atoms is determined in a fully relaxed geometry with the two bottom layers fixed. Periodic boundary conditions are applied in the two lateral directions to simulate the Cu(001) substrate. For the investigation of the bulk properties, periodic boundary conditions are applied in three dimensions with no atoms fixed. In the calculations, the cutoff radius for the interatomic potentials is set to 6.0 Å.

C. The energy barriers

Table II presents the calculated energy barriers for the exchange between a Co atom and a neighboring vacancy $E_{i\to j}^{\mathrm{Co,vac}}$, the shift of a Co-Cu dimer due to a vacancy jump $E_{i\to j}^{\mathrm{dim,vac}}$, the exchange of a Co and a Cu atoms $E_{i\to j}^{\mathrm{Co,Cu}}$, and the cyclic exchange of a Co-Cu-Cu trimer $E_{i\to j}^{\mathrm{trim}}$. The calculation results show that the energy barriers for Co migration into the deeper layers increase towards the bulk values. The bulk values are achieved for the migration into the sixth and deeper layers. Besides that, the imbalances between the energy barriers for the migration in the direction towards the surface and the migration in the other way around are also revealed. In the first three atomic layers, the energy barriers for Co migration towards the surface are higher by 0.018 eV up to 1.198 eV compared to those for the migration towards the bulk. Such imbalances are due to the different energies provided by the locations of a single Co atom as well as a single vacancy in the layers of Cu(001). Our calculations reveal that the energy due to the embedding of a Co atom in the first layer is higher by 0.451 eV compared to it due to the embedding in the second layer, while Co embedding in the second layer leads to an energy being higher than it is in the third layer by 0.054 eV. The calculated energy of the system of Cu(001) with a vacancy in the second layer is higher by 0.763 eV and 0.036 eV compared to those where a vacancy is located in the first and third layers, respectively. The energy of the system with a vacancy in the third layer is found to be higher by 0.011 eV than it is for a vacancy located in the fourth layer. These are in good qualitative agreement with the results reported in Refs. [43,45].

The presented calculation results suggest that the ring-exchange mechanism is not dominant in the interlayer migration of Co. The energy barriers for migration via the ring-exchange mechanism are much higher than the barriers for the

TABLE II. The calculated energy barriers of the interlayer migration via an exchange between a Co atom and a vacancy ($E_{i\to j}^{\mathrm{Co,vac}}$), the shift of a Co-Cu dimer due to the jump of a vacancy ($E_{i\to j}^{\mathrm{dim,vac}}$), a Co atom and Cu atoms ($E_{i\to j}^{\mathrm{Co,\,Cu}}$), as well as the cyclic exchange of a Co-Cu-Cu trimer ($E_{i\to j}^{\mathrm{trim}}$). The energies are presented in eV.

down					up				
$i \to j$	$E_{i\to j}^{\mathrm{Co,vac}}$	$E_{i\to j}^{\mathrm{dim,vac}}$	$E_{i\to j}^{\mathrm{Co,\,Cu}}$	$E_{i\to j}^{\mathrm{trim}}$	$i \to j$	$E_{i\to j}^{\mathrm{Co,vac}}$	$E_{i\to j}^{\mathrm{dim,vac}}$	$E_{i\to j}^{\mathrm{Co,\,Cu}}$	$E_{i\to j}^{\mathrm{trim}}$
$1 \to 2$	0.105	0.672	2.857	2.059	$2 \to 1$	1.303	1.726	3.308	2.510
$2 \to 3$	0.891	0.851	4.933	2.913	$3 \to 2$	0.909	1.759	4.987	2.967
$3 \to 4$	0.968		5.128	3.765	$4 \to 3$	0.965		5.135	3.772
$4 \to 5$	0.978		5.179	4.821	$5 \to 4$	0.978		5.179	4.821
bulk	0.981		5.188	4.827	bulk	0.981		5.188	4.827

TABLE III. The calculated formation energy of vacancies in the layers of Cu(001) E_j^{F}, the energy due to the interaction of a Co atom in the ith layer and a vacancy in the jth layer $\Delta_{i,j}$, the total energy barrier for Co migration due to the exchange with a vacancy $E_{\mathrm{A}\,i\to j}^{\mathrm{Co,vac}}$, and due to the shift of a Co-Cu dimer $E_{\mathrm{A}\,i\to j}^{\mathrm{dim,vac}}$. The energies are presented in eV.

down					up				
$i \to j$	E_j^{F}	$\Delta_{i,j}$	$E_{\mathrm{A}\,i\to j}^{\mathrm{Co,vac}}$	$E_{\mathrm{A}\,i\to j}^{\mathrm{dim,vac}}$	$i \to j$	E_j^{F}	$\Delta_{i,j}$	$E_{\mathrm{A}\,i\to j}^{\mathrm{Co,vac}}$	$E_{\mathrm{A}\,i\to j}^{\mathrm{dim,vac}}$
$1 \to 2$	1.312	0.104	1.521	1.948	$2 \to 1$	0.549	0.121	1.973	2.396
$2 \to 3$	1.276	0.129	2.296	2.256	$3 \to 2$	1.312	0.130	2.351	2.308
$3 \to 4$	1.265	0.131	2.364		$4 \to 3$	1.276	0.130	2.371	
$4 \to 5$	1.264	0.131	2.373		$5 \to 4$	1.265	0.131	2.374	
bulk	1.264	0.131	2.376		bulk	1.264	0.131	2.376	

vacancy-assisted Co shifts. Moreover, the energies required to realize the ring-exchange mechanism are considerably higher than the experimental value of activation energy of Co diffusion in Cu $E_{\mathrm{b}} = 2.22$ eV except for the migration from the first into the second layer.

Co migration via the vacancy mechanism is mainly due to the exchange between a Co atom and a neighboring vacancy. The migration due to the shift of a Co-Cu dimer due to a vacancy jump in general requires considerably higher energies compared to the Co-vacancy exchange. Considerably low-energy barriers for the Co-Cu shift are found only for the case where a vacancy jumps from the third into the first layer. Such shifts only provide the migration of Co into the second and the third layers. The vacancy-assisted migration into the deeper layers is due to the hopping of single Co atoms into vacancies.

To inspect the role of the vacancy mechanism in Co migration in Cu, the total energy barriers for the migration processes that involve the vacancy jump are determined. For this, the formation energy of a vacancy in different layers of Cu(001) is calculated. Two cases are considered. The first case is when the vacancy is formed in Cu(001) without the presence of Co. The second one is when a vacancy is formed adjacent to a Co atom in the neighboring layer. The difference of the formation energies that are obtained in these two cases gives the energy difference $\Delta_{i,j}$ that accommodates the interaction between a Co atom and a vacancy as described in Sec. IV A.

The calculated formation energy of the vacancies, the energy due to Co-vacancy interaction, and the energy barriers for Co vacancy-assisted migration are presented in Table III. The calculation results show that the formation energy of a subsurface vacancy decreases towards the bulk value. The bulk value is achieved for a vacancy that is located in the fifth and deeper layers. The energy due to the Co-vacancy interaction shows significant differences from the bulk value when the Co atom and the vacancy are located in the first two layers.

The total barriers for the vacancy-assisted Co interlayer migration are calculated by summing up the vacancy formation energy, the energy due to the Co-vacancy interaction, and the energy for the shift of a Co atom or a Co-Cu dimer due to the vacancy jump. The calculated total energy barriers for the migration via the vacancy mechanism are considerably lower than those for the migration via the ring mechanism. This confirms that the vacancy mechanism is the dominant mechanism in the Co interlayer migration in Cu(001). Moreover, the bulk value of the total barrier for the exchange between a Co atom and a vacancy $E_{\mathrm{A,\,bulk}}^{\mathrm{Co,vac}} = 2.376$ eV is closer to the experimental value of the activation energy of Co diffusion in bulk Cu $E_{\mathrm{b}} = 2.22$ eV than the other calculated bulk values of the energy barriers for the migration. Therefore our calculation leads to the conclusion that the Co-vacancy exchange is the main mechanism in Co diffusion in bulk Cu.

D. Calculation of Co distribution in Cu(001) layers

Based on the description of the model, the distribution of Co in the layers of the substrate is calculated. It is done by determining the rate of migration of Co atoms into each layer of Cu(001), which is described in the following paragraphs.

Since the embedding of Co into the first layer is assumed to take place immediately upon the landing of the deposited atoms on the hot Cu(001), the rate of embedding of Co atoms from the surface into the first layer equals the deposition rate F. The rate of the migration of Co atoms from the ith layer into the $j = i \pm 1$-th layer, $\nu_{i,j}$, is the sum of the rates of migration via different mechanisms,

$$\nu_{i,j} = \delta_{j,i\pm1}\left(\nu_{i,j}^{\mathrm{Co,vac}} + \nu_{i,j}^{\mathrm{dim,vac}} + \nu_{i,j}^{\mathrm{trim}}\right), \tag{8}$$

where $\delta_{\mathrm{i,k}}$ is the Kroenecker's delta, $\nu_{i,j}^{\mathrm{Co,vac}}$, $\nu_{i,j}^{\mathrm{dim,vac}}$ and $\nu_{i,j}^{\mathrm{trim}}$ are the rates of migration via Co-vacancy exchange, Co-Cu dimer shift, and Co-Cu-Cu trimer cyclic exchange, respectively. The rate of the migration via the direct Co-Cu exchange is neglected due to the high activation energy. For similar reasons, the rate of migration via the Co-Cu dimer shift $\nu_{i,j}^{\mathrm{dim,vac}}$ is neglected for the case of $\max\{i,j\} > 3$ and the rate of migration via the trimer cyclic exchange $\nu_{i,j}^{\mathrm{trim}}$ is neglected when $\max\{i,j\} > 2$. The rates $\nu_{i,j}^{\mathrm{Co,vac}}$, $\nu_{i,j}^{\mathrm{dim,vac}}$ and $\nu_{i,j}^{\mathrm{trim}}$ are calculated as follows:

$$\nu_{i,j}^{\mathrm{Co,vac}} = 4\nu_0 n_j^{\mathrm{vac}} \exp\left(-\frac{E_{i\to j}^{\mathrm{Co,vac}} + \Delta_{i,j}}{kT}\right), \tag{9}$$

$$\nu_{i,j}^{\mathrm{dim,vac}} = 4\nu_0^{\mathrm{dim}} n_{\mathrm{2\text{-}i+j}}^{\mathrm{vac}} \exp\left(-\frac{E_{i\to j}^{\mathrm{dim,vac}} + \delta_{\mathrm{i,2}}\Delta_{i,j}}{kT}\right), \quad \max\{i,j\} \leqslant 3, \tag{10}$$

$$\nu_{i,j}^{\mathrm{trim}} = 4\nu_0^{\mathrm{trim}} \exp\left(-\frac{E_{i\to j}^{\mathrm{trim}}}{kT}\right), \quad \max\{i,j\} \leqslant 2, \tag{11}$$

where the quantities $\nu_0 = 12.7$ THz and $\nu_0^{\mathrm{dim}} = 277.5$ THz are prefactors for the diffusion of Co adatoms and Co-Co dimers calculated in the framework of the classical transition state

theory [53]. The values that are used in the calculation are typical for jumps and exchanges of atoms on the Cu(001) surface [54]. The value of ν_0^{trim} is assumed to be equal to ν_0^{dim}. The factor n_j^{vac} is the vacancy concentration in the jth layer. It is determined using the formula

$$n_j^{\text{vac}} = \exp\left(-\frac{G_j^{\text{F}}}{kT}\right), \tag{12}$$

where

$$G_j^{\text{F}} \approx E_j^{\text{F}} - TS_j^{\text{F}}. \tag{13}$$

Here, G_j^{F} and S_j^{F} are the Gibbs free energy and the entropy for the formation of a vacancy in the jth layer, respectively. The Gibbs formation energy of vacancy formation is determined as follows.

The Gibbs free energy for the formation of a vacancy in the bulk region $G_{\text{bulk}}^{\text{F}}$ is determined by considering the difference between the calculated bulk value of the total energy barrier for the Co-vacancy exchange $E_{\text{A, bulk}}^{\text{Co,vac}} = 2.376$ eV and experimental value of the activation energy of Co bulk diffusion in Cu $E_{\text{b}} = 2.22$ eV, which is equal to 0.156 eV. This value is close to the value of $TS_{\text{bulk}}^{\text{F}}$ at 650 K, 0.148 eV, which is obtained by implementing the experimental value [42]. Thus this difference between $E_{\text{A, bulk}}^{\text{Co,vac}}$ and E_{b} is attributed to $TS_{\text{bulk}}^{\text{F}}$. The value of $G_{\text{bulk}}^{\text{F}}$ is obtained by subtracting $TS_{\text{bulk}}^{\text{F}} = 0.156$ eV from the calculated $E_{\text{bulk}}^{\text{F}}$, giving $G_{\text{bulk}}^{\text{F}} = 1.108$ eV. The Gibbs free energy of vacancy formation in the jth layer is determined by assuming $S_j^{\text{F}} = S_{\text{bulk}}^{\text{F}}$, which gives $G_j^{\text{F}} = E_j^{\text{F}} - (E_{\text{A, bulk}}^{\text{Co,vac}} - E_{\text{b}})$.

The rate of migration of Co atoms into the layers of Cu(001) is given by the following system of differential equations:

$$\begin{aligned}
\frac{\mathrm{d}n_1}{\mathrm{d}t} &= F - \nu_{1,2}n_1 + \nu_{2,1}n_2, \\
\frac{\mathrm{d}n_i}{\mathrm{d}t} &= \nu_{\text{i-1,i}}n_{\text{i-1}} + \nu_{\text{i+1,i}}n_{\text{i+1}} - (\nu_{\text{i,i-1}} + \nu_{\text{i,i+1}})n_i, \quad i > 1,
\end{aligned} \tag{14}$$

where n_i is the Co concentration in the ith layer of Cu(001). In our calculation, the interlayer migration in the first ten layers is considered. The deposition rate F is 0.2 ML min^{-1} for $0 \leqslant t \leqslant 30$ s and 0 for $t > 30$ s. The set of equations above are solved for $T = 650$ K, giving the distributions of Co in Cu(001) at the time when the deposition stops ($t = 30$ s, black-filled squares), at $t = 10$ minutes (red-filled circles), and at $t = 55$ minutes (blue-filled triangles) as presented in Fig. 6.

V. DISCUSSION

Our model provides the explanation for the features that are revealed by the experimental plots in Fig. 3. The calculated distributions presented in Fig. 6 reveal almost no Co atoms are embedded in the first layer, confirming the experimental observation. The low-energy barriers for the migration into the subsurface layers provide a significant Co migration from the first layer into the subsurface layers at 650 K. The considerable imbalances between the energy barriers for the migration from and into the first layer causes the rate of migration back into the first layer much lower than the migration into the layers below it.

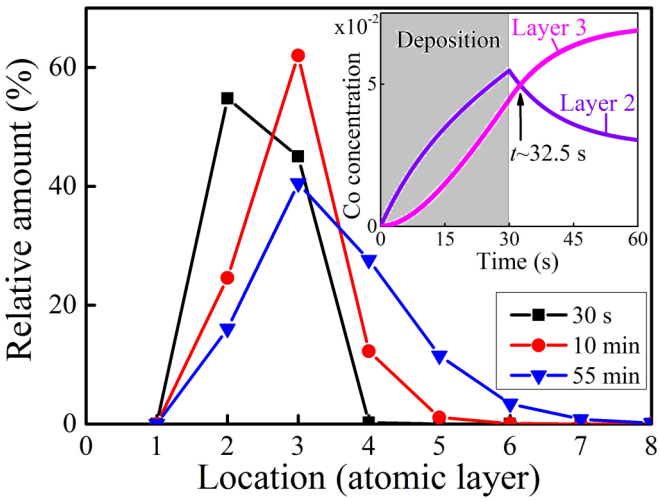

FIG. 6. The distributions of Co atoms in Cu(100) at 650 K for different time durations as calculated using Eq. (14). The black-filled squares, the red-filled circles, and the blue-filled triangles correspond to the time durations of 30 seconds, 10 minutes, and 55 minutes, respectively. The straight lines are guides to the eyes. (Inset) The calculated concentration of Co atoms in the second (the violet curve) and third (the magenta curve) layers for the first 60 seconds. During this period, the amount of Co in the other layers is negligible. The gray area indicates the time during the deposition. The arrow shows the time when the concentration in the third layer equals to the concentration in the second layer.

According to our calculation, the maximum of the distribution at the third layer, which is revealed by the experimental plot, is not achieved directly upon the deposition. As shown by the black-filled squares in Fig. 6, Co atoms are initially accumulated mainly in the second and third layers with the larger amount of them in the second layer. After the deposition stops, Co diffuses into the deeper layers where the rate of migration of Co atoms from the second layer into the third layer is higher than the migration the other way around due to the imbalances of interlayer migration energy barriers. As a result, the maximum of Co distribution shifts from the second into the third layer as shown by the distribution presented by the red-filled circles in Fig. 6. Our calculation predicts that at 650 K the shift of the distribution maximum takes place within less than 3 seconds after the deposition stops (see the inset in Fig. 6). Considering the experimental condition, the calculation result suggests that the distribution maximum at the third layer was obtained during the cooling down process when the temperature of the sample was still considerably high.

The calculated distribution presented by the blue-filled triangles in Fig. 6 reproduces the features and the profile of the experimental plots. This approves that our model is able to capture the essential physical mechanisms of the Co near-surface diffusion in Cu(001). Minor discrepancies between the experimental and the calculated distribution plots can be found, especially regarding the time scale. In our calculation, the distribution presented by the blue-filled triangles is achieved

around 50 min after the deposition stops provided the sample temperature is kept at 650 K, whereas such a time is somewhat shorter in the experiment. Nevertheless, this difference in the time scale is actually insignificant as explained in the following.

The difference between the time scale in the calculation and in the experiment is attributed mainly to the inaccuracies of the calculated energy barriers. Besides that, simplification of the assumptions that are applied in the calculation of the distribution can also have some consequences in time scales. Due to the exponential dependency of the atomic jump rates on the energy barriers, slight deviations of the calculated energy barriers from the actual values can induce some discrepancy between the time scale in the calculation and the experiment. For the diffusion via the vacancy mechanism, which has been concluded as the main mechanism for Co diffusion in Cu (see Sec. IV C), the inaccuracies of our calculated energy barriers can be estimated from the variation of the reported vacancy formation and migration energy. From the variation of the values presented in Refs. [39,41–44,55], our calculated energy barriers also could be slightly inaccurate by several percent. Such small inaccuracies might have induced an overestimated calculated time by one or two orders of difference to achieve the profile presented by the blue-filled triangles in Fig. 6. Based on this, the disagreement between the calculation and the experimental time scales is only a matter of small inaccuracies in the calculated energy barriers. Another factor that can contribute to the time scale difference are the assumptions that are applied in the calculation of the vacancy concentration. In the calculation using Eq. (12), the entropy of vacancy formation has been assumed to be equal to the bulk value for all layers while some deviations can be expected for the first few layers. In addition to this, the use of Eq. (12) to calculate the vacancy concentration assumes the sample to be in thermal equilibrium. In the actual experiment, a small temperature variation in the sample that is beyond the accuracy of our measurement could take place during the deposition. During the cooling down, the sample was actually in a quasithermal equilibrium considering the long cooling down time. Regarding the nonlinear relation between the vacancy concentration, the temperature, and the entropy for vacancy formation [56], the deviation from the thermal equilibrium and the variation of the entropy for vacancy formation in the first few atomic layers could induce a difference between the calculated rate of interlayer migration from the actual one. Thus an exact quantitative agreement regarding the time scale is related to the used approximation, which is not an important aspect of this study. The fact that the features and the profile of the experimental plots are well reproduced by our calculation is sufficient to validate our model.

VI. SUMMARY AND CONCLUSIONS

We have discussed the diffusion of single Co atoms in the near-surface region of Cu(001). This near surface diffusion provides the embedding of single Co atoms in the first few atomic layers of Cu(001) upon a deposition at 650 K. The distribution of the depth of location of single Co atoms in Cu(001) has been analyzed to study the details of the embedding process. The depth of location is determined using STM. The distribution reveals the largest amount of Co atoms in the third layer while only a negligible amount of Co atoms is in the first layer. All of these put in evidence that the value of diffusion parameters is depth dependent. A theoretical work has been performed to provide the explanation for the experimental results. A model that describes the embedding process into Cu(001) layers is proposed. The energy barriers for the diffusion of single Co atoms into the atomic layers of Cu(001) were calculated. It is found that the energy barriers for the diffusion into the first five atomic layers are lower than those in the deep region where the bulk values apply.

As an additional value of this presented work, STM has been used to determine the depth of location of buried impurity atoms where the resolution of one atomic layer is obtained. This demonstrates that STM can be a powerful technique for subsurface studies which require depth determination with very high resolution.

ACKNOWLEDGMENTS

This study is part of the research programme of the Foundation for Fundamental Research on Matter (FOM), which is part of the Netherlands Organisation for Scientific Research (NWO). S.V.K. and A.L.K. thank the Russian Foundation for Basic Research (RFBR 15-32-20560) for support.

[1] D. K. Reimann and J. P. Stark, Acta Metall. **18**, 63 (1970).
[2] R. E. Hanneman and T. R. Anthony, Acta Metall. **17**, 1133 (1969).
[3] D. L. Styris and C. T. Tomizuka, J. Appl. Phys. **34**, 1001 (1963).
[4] T. Hirone and H. Yakamoto, J. Phys. Soc. Jpn. **16**, 455 (1961).
[5] C. B. Pierce and D. Lazarus, Phys. Rev. **114**, 686 (1959).
[6] S. Kristyan and J. Giber, Surf. Sci. **224**, 476 (1989).
[7] R. S. Li and T. Koshikawa, Surf. Sci. **151**, 459 (1985).
[8] P. S. Ho, Surf. Sci. **72**, 253 (1978).
[9] J. Roth, W. Moller, D. B. Poker, and K. Wittmaack, Nucl. Instrum. Methods B **13**, 409 (1986).
[10] J. F. Mojica and L. L. Levenson, Surf. Sci. **59**, 447 (1976).
[11] O. L. J. Gijzeman, F. C. Schouten, and G. A. Bootsma, Surf. Sci. **71**, 174 (1978).
[12] F. Bezuidenhout, J. D. Plessis, and P. E. Viljoen, Surf. Sci. **171**, 392 (1986).
[13] U. Ramsperger, A. Vaterlaus, P. Pfäffli, U. Maier, and D. Pescia, Phys. Rev. B **53**, 8001 (1996).
[14] T. Siahaan, O. Kurnosikov, H. J. M. Swagten, and B. Koopmans, Phys. Rev. B **90**, 165419 (2014).
[15] C. Nagl, E. Platzgummer, M. Schmid, P. Varga, S. Speller, and W. Heiland, Phys. Rev. Lett. **75**, 2976 (1995).
[16] J. Fassbender, R. Allenspach, and U. Dürig, Surf. Sci. **383**, L742 (1997).

[17] T. Bernhard, R. Pfandzelter, and H. Winter, Nucl. Instrum. Methods Phys. Res., Sect. B **203**, 111 (2003).
[18] F. Nouvertné, U. May, M. Bamming, A. Rampe, U. Korte, G. Güntherodt, R. Pentcheva, and M. Scheffler, Phys. Rev. B **60**, 14382 (1999).
[19] R. van Gastel, R. van Moere, H. J. W. Zandvliet, and B. Poelsema, Surf. Sci. **605**, 1956 (2011).
[20] C. Lee, G. T. Barkema, M. Breeman, A. Pasquarello, and R. Car, Surf. Sci. Lett. **306**, L575 (1994).
[21] R. Pentcheva, Appl. Phys. A **80**, 971 (2005).
[22] M. Hansen and K. Anderko, *Constitution of Binary Alloys* (McGraw-Hill, New York, 1958).
[23] T. Nishizawa and K. Ishida, Bull. Alloy Phase Diagram **5**, 161 (1984).
[24] R. Döhl, M.-P. Macht, and V. Naundorf, Phys. Status Solidi A **86**, 603 (1984).
[25] A. A. Itckovich, B. S. Bokstein, and A. O. Rodin, Mater. Lett. **135**, 241 (2014).
[26] A. Weismann, M. Wenderoth, S. Lounis, P. Zahn, N. Quaas, R. G. Ulbrich, P. H. Dederichs, and S. Blügel, Science **323**, 1190 (2009).
[27] H. Prüser, M. Wenderoth, A. Weismann, and R. G. Ulbrich, Phys. Rev. Lett. **108**, 166604 (2012).
[28] P. Wahl, A. P. Seitsonen, L. Deikhöner, M. A. Schneider, and K. Kern, New. J. Phys. **11**, 113015 (2009).
[29] O. Kurnosikov, J. T. Kohlhepp, and W. J. M. de Jonge, Europhys. Lett. **64**, 77 (2003).
[30] O. Kurnosikov, J. T. Kohlhepp, and W. J. M. de Jonge, Surf. Sci. **566-568**, 175 (2004).
[31] O. A. O. Adam, O. Kurnosikov, J. T. Kohlhepp, H. J. M. Swagten, W. J. M. de Jonge, and B. Koopmans, Jpn. J. Appl. Phys. **45**, 2014 (2006).
[32] C. G. Zimmermann, M. Yeadon, K. Nordlund, J. M. Gibson, R. S. Averback, U. Herr, and K. Samwer, Phys. Rev. Lett. **83**, 1163 (1999).
[33] M. F. Crommie, C. P. Lutz, and D. M. Eigler, Science **262**, 218 (1993).
[34] M. F. Crommie, C. P. Lutz, D. M. Eigler, and E. J. Heller, Physica D **83**, 98 (1995).
[35] M. F. Crommie, C. P. Lutz, D. M. Eigler, and E. J. Heller, Surf. Sci. **361/362**, 864 (1996).
[36] M. F. Crommie, J. Electron Spectrosc. Relat. Phenom. **109**, 1 (2000).
[37] S. Lounis, P. Zahn, A. Weismann, M. Wenderoth, R. G. Ulbrich, I. Mertig, P. H. Dederichs, and S. Blügel, Phys. Rev. B **83**, 035427 (2011).
[38] M. E. Glicksman, *Diffusion in Solids: Field Theory, Solid-State Principles, and Applications* (Wiley, New York, 2000).
[39] R. O. Simmons and R. W. Balluffi, Phys. Rev. **129**, 1533 (1963).
[40] R. R. Bourassa and B. Langeler, J. Phys. F **6**, 1405 (1976).
[41] A. S. Berger, S. T. Ockers, and R. W. Siegel, J. Phys. F **9**, 1023 (1979).
[42] P. A. Varotsos and K. D. Alexopoulos, *Thermodynamics of Point Defects and Their Relation with Bulk Properties* (North-Holland, Amsterdam, 1986).
[43] C. Wang, C. Tang, J. Su, Y. Zhang, Q. Sun, and Y. Jia, Solid State Sci. **13**, 1989 (2011).
[44] H. B. Huntington and F. Seitz, Phys. Rev. **61**, 325 (1942).
[45] N. A. Levanov, V. S. Stepanyuk, W. Hergert, D. I. Bazhanov, P. H. Dederichs, A. A. Katsnelson, and C. Massobrio, Phys. Rev. B **61**, 2230 (2000).
[46] V. S. Stepanyuk, D. V. Tsivline, D. I. Bazhanov, W. Hergert, and A. A. Katsnelson, Phys. Rev. B **63**, 235406 (2001).
[47] H. Jónsson, G. Mills, and K. W. Jacobsen, in *Classical and Quantum Dynamics in Condensed Phase Simulation*, edited by B. J. Berne, G. Giccotti, and D. F. Coker (World Scientific, Singapore, 1998), Chap. 16, p. 385.
[48] F. Cleri and V. Rosato, Phys. Rev. B **48**, 22 (1993).
[49] N. N. Negulyaev, V. S. Stepanyuk, P. Bruno, L. Diekhöner, P. Wahl, and K. Kern, Phys. Rev. B **77**, 125437 (2008).
[50] S. V. Kolesnikov, A. L. Klavsyuk, and A. M. Saletsky, Phys. Rev. B **79**, 115433 (2009).
[51] S. V. Kolesnikov, A. L. Klavsyuk, and A. M. Saletsky, Surf. Sci. **612**, 48 (2013).
[52] S. V. Kolesnikov, A. L. Klavsyuk, and A. M. Saletsky, Eur. Phys. J. B **86**, 399 (2013).
[53] S. A. Dokukin, O. V. Drozdov, S. V. Kolesnikov, and A. M. Saletsky, Phys. Solid State **55**, 1505 (2013).
[54] G. Boisvert and L. J. Lewis, Phys. Rev. B **56**, 7643 (1997).
[55] D. A. Andersson and S. I. Simak, Phys. Rev. B **70**, 115108 (2004).
[56] H. Mehrer, *Diffusion in Solids: Fundamentals, Methods, Materials, Diffusion-Controlled Processes* (Springer, Berlin, 2007).